

SPH simulations of Shakura-Sunyaev instability at intermediate accretion rates

V. Teresi¹ *, D. Molteni¹ and E. Toscano¹

¹*Dipartimento di Fisica e Tecnologie Relative, Università di Palermo, Viale delle Scienze, Palermo, 90128, Italy*

17 January 2019

ABSTRACT

We show that a standard Shakura-Sunyaev accretion disc around a black hole with an accretion rate \dot{M} lower than the critical Eddington limit does show the instability in the radiation pressure dominated zone. We obtain this result performing time-dependent simulations of accretion disks for a set of values of α and \dot{M} . In particular we always find the occurrence of the collapse of the disc: the instability develops always towards a collapsed gas pressure dominated disc and not towards the expansion. This result is valid for all initial configurations we tested. We find significant convective heat flux that increases the instability development time, but is not strong enough to inhibit the disc collapse. A physical explanation of the lack of the expansion phase is proposed considering the role of the radial heat advection. Our finding is relevant since it excludes the formation of the hot comptonizing corona –often suggested to be present– around the central object by the mechanism of the Shakura-Sunyaev instability. We also show that, in the ranges of α and \dot{M} values we simulated, accretion disks are crossed by significant amplitude acoustic waves.

Key words: accretion, accretion disks — black hole physics — hydrodynamics — instabilities

1 INTRODUCTION

This work concerns the possibility of occurrence, stated by Shakura and Sunyaev (Shakura & Sunyaev 1976), of an instability in the α -discs when the radiation pressure dominates, i.e. in the so-called A zone. Shakura and Sunyaev demonstrated the existence of thermal instabilities connected with a difference between Q_- and Q_+ , i.e. the energy emitted per unit area of the disc and the rate of energy-generation in the disc. The problem of the existence and outcome of the Shakura-Sunyaev instability is important in accretion disc physics because it affects the model of the origin of the comptonization cloud around some compact objects whose spectra contain a significant part in the X-ray band. The idea of a hot gas cloud, called ‘comptonization cloud’, around the disc region close to the compact object, where photons are pushed towards high frequencies by the Compton scattering with electrons, is one of the most common ways to explain the spectral behavior in the X band (Sunyaev & Titarchuk 1980). In general, the outcome of the Shakura-Sunyaev instability is guessed to be the formation of a hot cloud around the internal disc region, in which comptonization could happen (Shapiro et al. 1976).

Some authors already studied the problem of the α -disc time evolution. In 1984 Taam and Lin found that the local Shakura and Sunyaev stability analysis is confirmed by global time-dependent simulations of the canonical disc. The instability appears and gives rise to luminosity fluctuations or bursts (Taam & Lin 1984). Taam and Lin’s result is similar to ours despite of the one-dimensional feature of their simulations (whereas we perform two-dimensional axisymmetric simulations). In 1987 Eggum et al. found that an α -disc, at sub-Eddington accretion rates, develops the Shakura-Sunyaev instability and, as a consequence of that, collapses in a cold thin sheet (Eggum et al. 1987). In 1998 Fujita and Okuda simulated a radiation pressure dominated α -disc in the subcritical accretion rate regime and found that it is thermally stable (Fujita & Okuda 1998). They analyzed the disc structure and found that it corresponds to the configuration of the slim accretion disc model (Abramowicz et al. 1988). In this model, even if the disc is radiation pressure and electron-scattering dominated, the equilibrium structure is thermally stable, as a consequence of an advective radial heat flux that is dominant with respect to the vertical radiative heat flux. The cases we present are different, since the structure of the disks we simulated is close to the α -model configuration, rather than to the slim accretion disc structure.

* E-mail: vteresi@unipa.it (VT)

In all the mentioned 2D works the evolution of the system has been simulated only for short time-scales, so their authors cannot exclude they detect only a transient behavior. In 2001 Agol et al., by performing local two-dimensional hydrodynamic simulations, showed that, for vertically integrated dissipation rate proportional to the vertically integrated total pressure, i.e. in the Shakura-Sunyaev model hypothesis, the thermal instability develops (Agol et al. 2001). The result of this instability is generally the disc collapse. Only if a strong enough initial increase of the local radiation energy density is given to the disc, there is an expansion, that the authors cannot follow because a large amount of matter is pushed out of the simulation region. In our simulations we confirm the results obtained by Eggum and by Agol. Furthermore our studies can follow the system evolution on a much larger time-scale and therefore give stronger relevance to the collapse result. We can also say that the post collapse phase is very long, at least $4.5 \cdot 10^5 \frac{R_g}{c}$ (where R_g is the Schwarzschild gravitational radius of the black hole and c is the light speed). We also suggest that the convective (in z and r directions) energy transport in the disc may have a twofold role: 1) to increase the time-scale of the collapse instability; 2) to inhibit the expansion instability.

2 THE PHYSICAL MODEL

The time dependent equations describing the physics of accretion disks are well known. They include: mass conservation

$$\frac{D\rho}{Dt} = -\rho \operatorname{div} \vec{v} \quad (1)$$

radial momentum conservation

$$\rho \frac{Dv_r}{Dt} = -\rho \frac{\lambda^2}{r^3} + g_r + (\operatorname{div} \vec{\sigma})_r + f_r \quad (2)$$

vertical momentum equation

$$\frac{Dv_z}{Dt} = -\frac{1}{\rho} \frac{dP}{dz} - g_z + f_z \quad (3)$$

energy balance

$$\rho \frac{D}{Dt} (E + \frac{1}{2}v^2) = \vec{v} \cdot \vec{F} \rho + \operatorname{div}(\vec{v} \vec{\sigma}) - \operatorname{div} \vec{F} \quad (4)$$

Here $\frac{D}{Dt}$ is the comoving derivative, \vec{F} is the radiation flux, given by:

$$\vec{F} = -\frac{c}{3\rho(k + \sigma_T)} \vec{\nabla} E_{rad} \quad (5)$$

k and σ_T are the free-free absorption and Thomson scattering coefficients, E_{rad} is the radiation energy per unit volume, \vec{f} is the radiation force, given by:

$$\vec{f} = \rho \frac{k + \sigma_T}{c} \vec{F} \quad (6)$$

λ is the angular momentum per unit mass, $E = \epsilon + \frac{E_{rad}}{\rho}$ is the total internal energy per unit mass, including gas and radiation terms, $\vec{\sigma}$ is the viscosity stress tensor. The component of $\vec{\sigma}$ that is important in accretion disks is the r - ϕ one, given by:

$$\sigma_{r\phi} = \nu \rho r \frac{d\omega}{dr} \quad (7)$$

$\nu = \alpha v_s H$ is the kinematic viscosity, α is the viscosity parameter of the Shakura-Sunyaev model, v_s is the local sound speed, H is the disc vertical thickness, ω is the local angular velocity and the other terms have the usual gas dynamic meaning.

The gravitational force produced by the black hole is given by the well-known pseudo-newtonian formula by Paczynski & Wiita (1980):

$$\vec{F} = -\frac{GM}{(R - R_g)^2} \frac{\vec{R}}{R} \quad (8)$$

where R_g is the Schwarzschild gravitational radius of the black hole, given by:

$$R_g = \frac{2GM}{c^2} \quad (9)$$

and M is the black hole mass.

We adopt the local thermal equilibrium approximation for the radiation transfer treatment. However this assumption does not affect our conclusions.

3 THE NUMERICAL METHOD AND THE SIMULATIONS PERFORMED

We set up a new version of the Smoothed Particles Hydrodynamics (SPH) code in cylindrical coordinates, for axis symmetric problems. We remind that SPH is a lagrangean interpolating method. Recently it has been shown it is equivalent to finite elements with sparse grid nodes moving along the fluid flow lines (Dilts 1996). For a detailed account of the SPH algorithm see Monaghan (1985). For cylindrical coordinates implementation see Molteni et al. (1998); Chakrabarti & Molteni (1993). Our code includes viscosity and radiation treatment. Let us note that -in general- a lagrangean code is better suited to capture convective motions than eulerian codes. With the same spatial accuracy (cell size equal to particle size) the SPH particle motion is tracked with great accuracy, i.e. the particle size may be large but its trajectory can be still determined 'exactly'. To integrate the energy equation we adopted the splitting procedure. In the LTE condition the radiation energy density changes according to the well known diffusion equation given by:

$$\frac{\partial E_{rad}}{\partial t} = -\operatorname{div} \vec{F} = \vec{\nabla} \cdot \left(\frac{c}{3\rho\kappa_{tot}} \vec{\nabla} E_{rad} \right) \quad (10)$$

where $\kappa_{tot} = k + \sigma_T$.

In cylindrical coordinates r, z :

$$\frac{\partial E_{rad}}{\partial t} = \frac{c}{r} \frac{\partial}{\partial r} \left(\frac{r}{3\rho\kappa_{tot}} \frac{\partial E_{rad}}{\partial r} \right) + \frac{c}{r} \frac{\partial}{\partial z} \left(\frac{r}{3\rho\kappa_{tot}} \frac{\partial E_{rad}}{\partial z} \right) \quad (11)$$

The SPH-version of the radiation transfer term is given following the criteria by Brookshaw (1994). The cylindrical coordinate version is given by:

$$\left(\frac{\partial E}{\partial t} \right)_i = \frac{1}{r_i} \sum_{j=1}^N \frac{m_j}{r_j} \left(\frac{E_i - E_j}{\rho_j} \right) D_{ij} \frac{\mathbf{R}_{ij}}{R_{ij}^2} \cdot \vec{\nabla}_i W_{ij} \quad (12)$$

where for clarity we did not put the subscript *rad* in E_{rad} and where:

$$D_{ij} = \left(\frac{cr_i}{3\rho_i\kappa_{tot_i}} + \frac{cr_j}{3\rho_j\kappa_{tot_j}} \right), \quad \mathbf{R}_{ij} = (r_i - r_j, z_i - z_j) \quad (13)$$

This formula can be obtained by the same procedure explained by Brookshaw, but taking into account that -in cylindrical coordinates- the particles masses are defined as $m_k = 2\pi \rho_k r_k \Delta r_k \Delta z_k$, that explains the further division by r_j in the term $\frac{m_j}{r_j}$.

The reference units we use are R_g , for length values, and R_g/c for time values.

We performed several simulations, the ones commented here had the following parameter values:

a) $\alpha = 0.01$, $\dot{M} = 0.7$, domain $R_1 - R_2 = 3 - 300$, $h = 0.3$;

b) $\alpha = 0.1$, $\dot{M} = 0.3$, domain $R_1 - R_2 = 3 - 200$, $h = 0.5$;

c) $\alpha = 0.01$, $\dot{M} = 0.7$, domain $R_1 - R_2 = 42 - 58$, $h = 0.04$;

where \dot{M} is in units of \dot{M}_E and \dot{M}_E is the critical accretion rate. For all cases the central black hole mass is $M = 10 M_\odot$. The spatial resolution we adopt is h . In the case 'a' we have $N = 29704$ particles at time $t = 0$.

We used a variable h procedure (Nelson & Papaloizou 1994). The h values above reported are the initial ones. In our procedure, in order to have a not too small particle size (and therefore not too great CPU integration times), we put a floor for the h values: h is chosen as the maximum between the value given by the variable h procedure itself and $1/10$ of the disc vertical half thickness. So we have nearly 10 particles along the disc half thickness even in the collapsed region. This floor was not adopted for the case 'c' since we already have a good resolution with a not exceeding number of particles ($N = 67518$).

The boundary conditions of the simulations are not fixed: as the SPH particles move around, the simulation region follows the form assumed by the disc and the values of the physical variables at the boundary of the disc are the values that characterize the boundary particles at a certain time.

The spatial extension of the initial configuration is decided by establishing a radial range of physical interest and a vertical extension given by the disc thickness of the Shakura-Sunyaev model.

For radiation, the boundary conditions we used are based on the assumption of the black-body emission and particularly on the Brookshaw approximation (Brookshaw 1994). At every time step boundary particles are identified by geometrical criteria (the particle having the maximum absolute value of z in a vertical strip of radial width given by h is a boundary particle). The boundary particle loses its thermal energy according to the formula given by Brookshaw (that is an approximation of the diffusion equation at the single particle level), that states the particle cooling rate proportional to

$$\frac{QT}{h^2} \quad (14)$$

where

$$Q = \frac{4acT^3}{3\rho\kappa_{tot}} \quad (15)$$

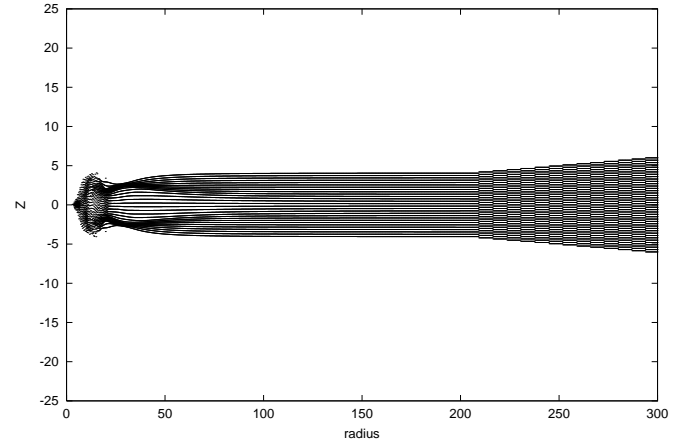


Figure 1. The r - z profile of the disc of case 'a' is shown at the time $t = 282 R_g/c$. Every SPH particle is represented by a small dot. On the x axis the r values in units of R_g are represented. On the y axis the z values in units of R_g are represented.

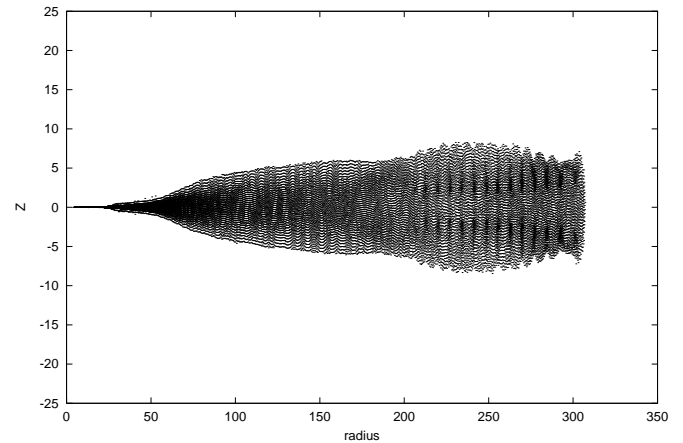


Figure 2. The r - z profile of the same disc case 'a' at the time $t = 12000 R_g/c$ is shown.

In all our simulations the boundary particles never reach an optical thickness lower than 10.

Let us now comment the results of our study referring to the figures of the simulation data.

Fig. 1 shows the disc structure for the case 'a' at the adimensional time $t = 282$. The disc profile shows the Z height of the disc, constant along the A zone. In this figure it is evident an initial large convective motion in the disc in a region close to the black hole.

Fig. 2 shows the same disc at the larger time $t = 12000$. The collapsed zone is clearly shown.

In Fig. 3, the ratio P_{rad}/P_{gas} at the times $t = 282$ and $t = 12000$ is shown, exhibiting evidence of the collapse.

Fig. 4 shows that the disc luminosity is steadily decreasing from the initial theoretical value to much lower values due to the lower temperature reached by the collapsed A zone.

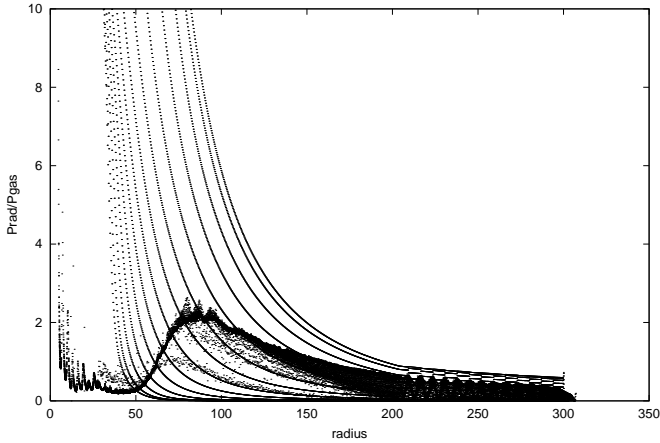


Figure 3. The ratio P_{rad}/P_{gas} at the times $t = 282$ and $t = 12000$ is shown. On the x axis the r values in units of R_g are represented. The configuration at the later time, collapsed, exhibits a gas pressure dominated zone up to $r = 70R_g$, whereas the other configuration, at an earlier time, shows that, up to $150 R_g$, the disc is radiation pressure dominated.

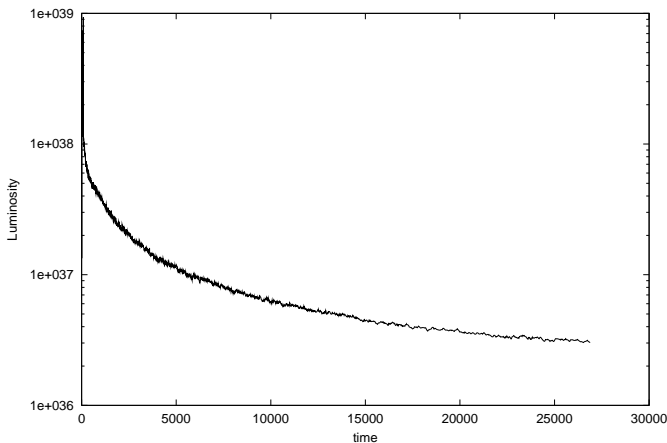


Figure 4. The time behavior of the disc luminosity is shown. On the x axis the time values in units of R_g/c are represented. On the y axis the luminosity values in units of $erg sec^{-1}$ are represented.

Case 'b' has a larger h and a lower number of particles and it was possible to follow on the simulation up to the large time $t = 680000$. The $r - z$ distribution of the disc particles is very similar to case 'a'.

We show in Fig. 5 the luminosity of this disc versus time. It is apparent that the luminosity has a large decrease during the collapse going down from a peak at $L = 6.5 \cdot 10^{37} erg sec^{-1}$ to $L = 8.5 \cdot 10^{35} erg sec^{-1}$. After the collapse the disc luminosity has a slow increase. Nearly after the time $t = 4.8 \cdot 10^5$ (corresponding to physical time $t = 48 sec$, for our parameters) the luminosity reached an average value of $L = 3 \cdot 10^{36} erg sec^{-1}$ and starts to show a strong flaring activity with luminosity reaching values up to $L = 1.6 \cdot 10^{37} erg sec^{-1}$. Obviously the possibility of a 'recharge' of the inner zone is to be expected and has been

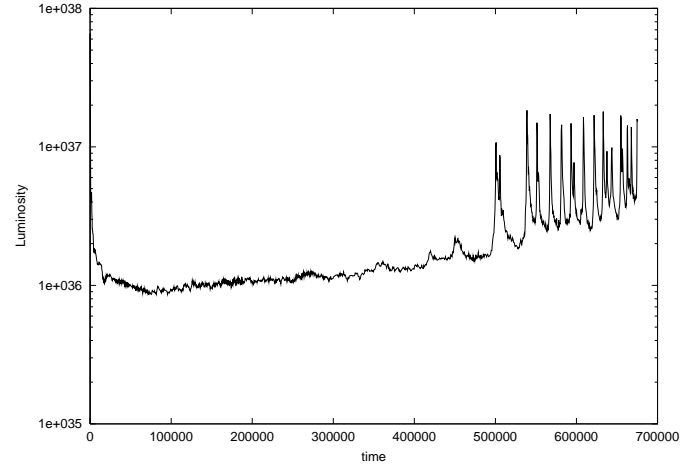


Figure 5. The time behavior of the disc luminosity is shown for the disc of case 'b'.

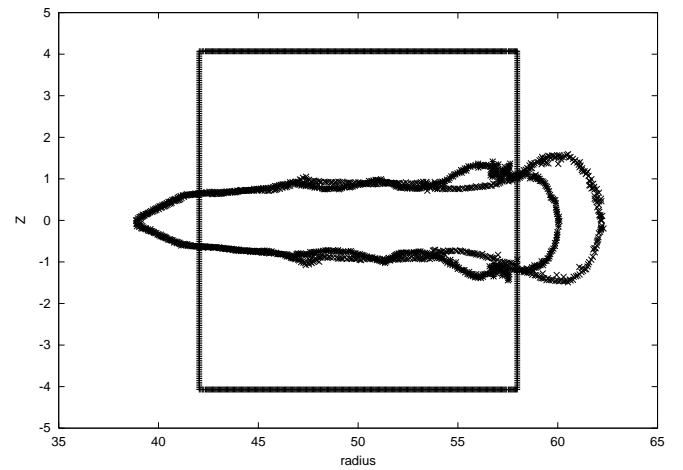


Figure 6. The border particles of the disc case 'c' are shown at the times $t = 0$ (vertical crosses), $t = 20000 R_g/c$ (diagonal crosses) and $t = 22400 R_g/c$ (asterisks).

guessed by Eggum and Agol, but -up to now- it was not given any estimate of the time-scale involved. It has to be noted that the refilling time-scale is definitely shorter than the radial viscous drift time-scale $t_{drift} = r^2/\nu$ as derived from the canonical disc structure.

In the 'c' case we simulated a small sector of the disc in the radiation pressure dominated zone with a very accurate spatial resolution. This case is similar to the Agol's case 1 (Agol et al. 2001), with nearly the same disc parameters and numerical resolution (the finest grid used for their case 1 is a 256×256 one, we have 67518 particles). We also obtained a vertical collapse instability of the disc and no expansion.

Fig. 6 shows the $r - z$ profiles at times $t = 20000$ and $t = 22400$ of the collapsing disc, compared with the disc profile in the initial configuration. The collapsed structure is completely gas pressure dominated. In the figure is also apparent the fact that there are waves travelling along the disc.

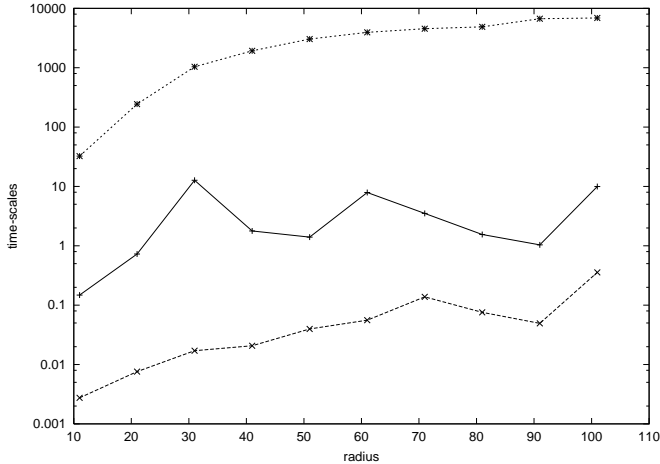


Figure 7. The radiative, convective and heating time-scales, ordered from the bottom to the top of the figure, are shown versus r . On the y axis the time values in units of R_g/c are represented.

During the simulations, we also calculate the z -averaged convective and advective heat fluxes at different values of r . With 'convective flux' we mean the heat flux along the z -direction due to the vertical motion of the gas, whereas with 'advective flux' we mean the heat flux along the r -direction due to the radial motion of the gas. The main time-scales involved in our problem are defined as follows.

The mean convection time-scale is $t_{conv} = \frac{\epsilon H}{F_{conv}}$, where F_{conv} is the z -averaged convective heat flux and ϵ is the total energy density. The mean radiation diffusion time-scale is $t_{rad} = \frac{\epsilon_r H}{F_{rad}}$, where F_{rad} is the z -averaged radiative heat flux and ϵ_r is the radiation energy density. The mean heating time-scale is $t_{heat} = \frac{dE_{rot}}{\tau_{r\phi} \frac{d\omega}{dr} dr}$, where dE_{rot} is the rotational energy of the disc ring between r and $r + dr$, $\tau_{r\phi}$ is the z -averaged viscosity stress and ω is the local angular velocity of the disc.

Fig. 7 shows the mentioned time-scales evaluated at different radii $r = 10 - 100 R_g$ for case 'b', after time $t = 10^5$.

From the comparison among the evaluated three time-scales it is clear that the convection time-scale is -in general- intermediate between the other two time-scales, i.e. the convection time-scale is greater than the vertical radiation diffusion time-scale and smaller than the heating time. So we can say that the vertical convective heat transfer may have a significant role in the vertical redistribution of the generated heat.

The role of the advection (radial transport) appears more relevant than the (vertical) convection. The time variation of the convective, advective and radiative fluxes is oscillatory and the oscillation frequency is close to the local keplerian frequency (Figs. 8 and 9).

The approximate equality between the flux oscillation and keplerian rotation frequencies is explainable if one assumes that the flux oscillation is due to the propagation of an acoustic wave in the disc. Milsom and Taam already showed that accretion disks are crossed by acoustic waves (Milsom & Taam 1996, 1997). In the limit of negligible viscosity and advection and for propagation direction per-

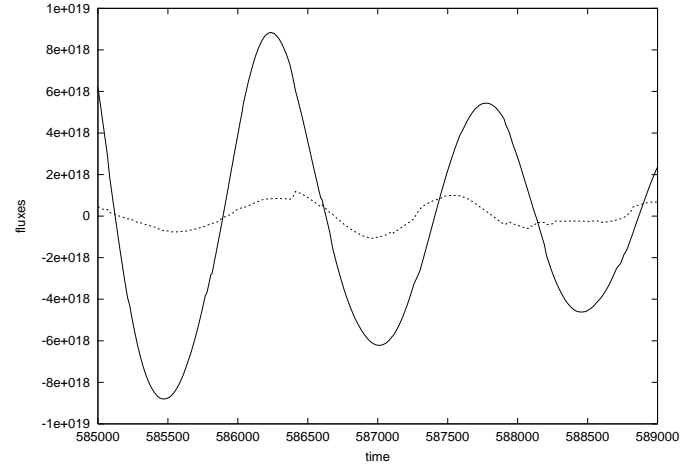


Figure 8. The convective and advective fluxes at $r = 30 R_g$ are shown versus time. On the y axis the fluxes values in units of $erg \ sec^{-1} \ cm^{-2}$ are represented. The dashed line represents the convective flux behavior, whereas the continuous one refers to the advective flux.

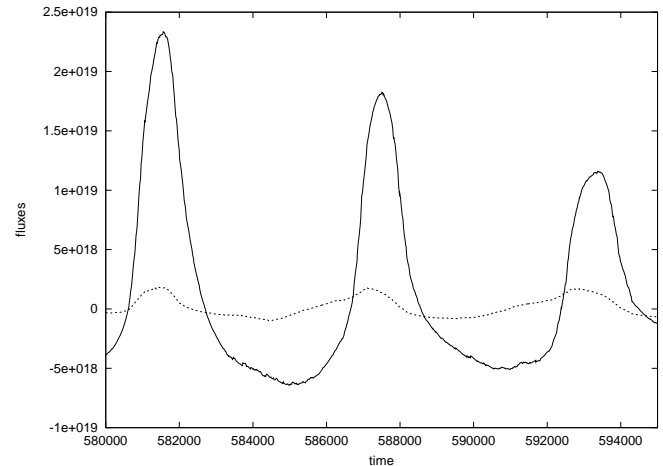


Figure 9. The convective and advective fluxes at $r = 80 R_g$ are shown versus time. On the y axis the fluxes values in units of $erg \ sec^{-1} \ cm^{-2}$ are represented. The dashed line represents the convective flux behavior, whereas the continuous one refers to the advective flux.

pendicular to the disc rotation axis, it is possible to have an analytical formula for the wave frequency. The dispersion relation for these waves is given by $\omega^2 = k^2 + K^2 v_s^2$ (Chandrasekhar 1961), where ω is the angular frequency of the wave, K is the wave number and k is the so-called local epicycle frequency, given by $k^2 = 2 \frac{\Omega}{r} \frac{d}{dr}(r^2 \Omega)$, where Ω is the local angular velocity of the disc. k is in general close to the local keplerian angular velocity. Therefore the fact that the waves frequencies and the keplerian angular velocities are close is a suggestion of the acoustic origin of such waves in accretion disks.

Finally, the waves we obtain have amplitudes that remain roughly constant in time. No other kind of disc structure variability is present.

We may add that the wave phenomenon appears -at different intensity levels- in all cases we examined. We never obtained a monotonic regular radial speed as the Shakura-Sunyaev model predicts.

4 DISCUSSION

Here we discuss two items : the absence of the expansion instability and the refilling of the inner zone of the disc.

The origin of the instability in radiation pressure dominated zone is clear, but it is not clear why the preferred evolution is towards the collapsed state and not towards the expanded one. At subcritical accretion rates, i.e. in our accretion rate regimes, the expansion instability never occurs. We suggest that this result can be due to two effects: the enhanced cooling in the expansion branch and the significant role of advection.

If the disc evolved towards the expansion instability the disc density would go down and therefore also its optical thickness. The basic LTE approximation, under which the disc model is built, breaks down; the disc can then radiate its energy content more quickly than it is heated by its viscosity. In our view the role of convection and advection may also contribute to reduce the expansion instability, but not the collapse instability. This mechanism has been considered capable to reduce the Shakura-Sunyaev instability. It is known that such a transfer should be present in accretion disks (Bisnovaty-Kogan & Blinnikov 1977; Fujita & Okuda 1998; Shakura et al. 1978), as a result of the entropy gradient associated with the radiation field in thermal equilibrium with the gas in the accretion disc. This gradient assumes a very large value when the temperature distribution is determined only by the radiative heat transfer and the viscous energy production rate. Following Bisnovaty-Kogan and Blinnikov analysis, the vertical convective motion and the consequent vertical heat transfer have, therefore, the role of producing an isentropic z structure. If we indicate with F_{conv} the vertical convective heat flux, the equation of the vertical heat transfer is, in presence of convection:

$$-\frac{d}{dz}(F_{rad} + F_{conv}) + \eta(r \frac{d\omega}{dr})^2 = 0 \quad (16)$$

where F_{rad} is the standard radiative flux. So we have a heat flux whose value has been enhanced from F_{rad} to:

$$F_{tot} = F_{rad} + F_{conv} = F_{rad}(1 + \frac{F_{conv}}{F_{rad}}) = fF_{rad} \quad (17)$$

where

$$f = 1 + \frac{F_{conv}}{F_{rad}} \quad (18)$$

It has been demonstrated that this enhancement of the vertical heat flux by a factor f produces an increase of the instability development time by the same factor f (Shakura et al. 1978). From our simulations we obtain that, in the parameter range we explored, f is always less than 2. Such a small value of f does not increase significantly the instability development time. However the advected radial heat is not taken into account in the calculations of Bisnovaty-Kogan & Blinnikov (1977); Shakura et al. (1978).

Figs. 10 and 11 show the radial and vertical speeds of

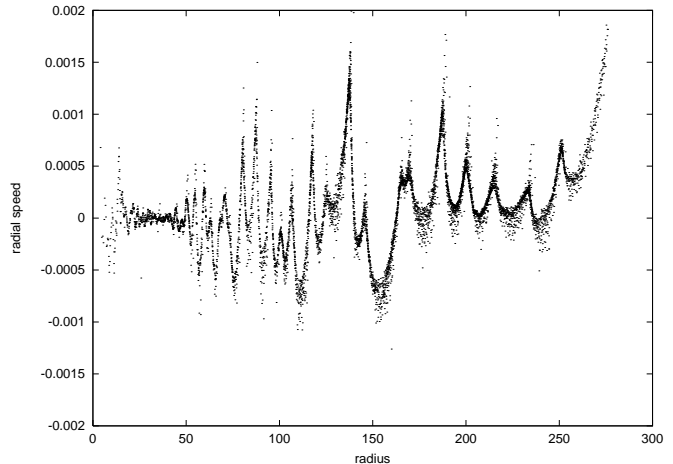


Figure 10. The radial speed of the disc parcels is shown versus r . On the y axis the speed values in adimensional units are represented.

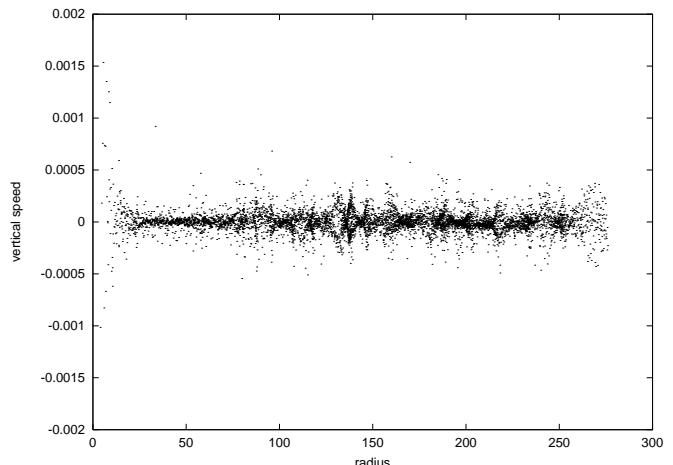


Figure 11. The vertical speed of the disc parcels is shown versus r . On the y axis the speed values in adimensional units are represented.

the disc parcels versus r . It is clearly apparent from Figs. 8, 9, 10 and 11 that the radial flux is greater than the vertical one.

As the radial heat flux assumes a significant value, the heat produced at a certain radius is carried away from that point of the disc where it had the possibility to produce the expansion instability. Furthermore this advection helps the cooling of the disc towards the collapsed configuration of the instability.

We obtain values of the radial heat flux that are large with respect to the vertical convective flux. Therefore we propose that the absence of the disc expansion may be due also to the role of the radial advective heat transfer.

As regards the collapse instability development times, we have compared the theoretical values with the ones calculated from the luminosity time behavior: we see that, when the disc collapses, its luminosity decreases very

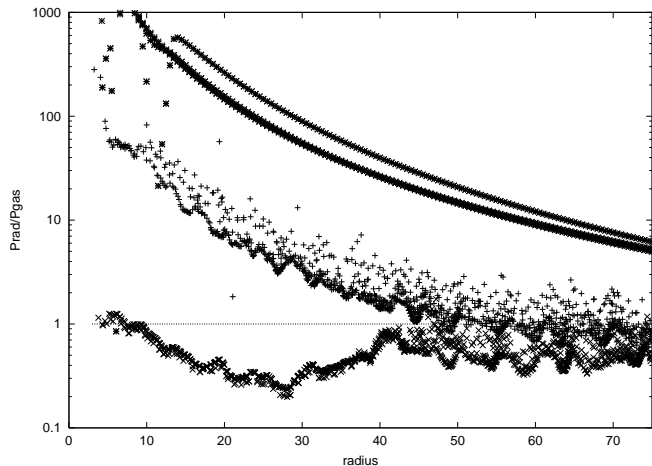


Figure 12. The ratio P_{rad}/P_{gas} in the initial configuration (asterixes) and at the times $t = 10^5$ (diagonal crosses) and $t = 6 \cdot 10^5$ (vertical crosses) is shown. The initial configuration, in the shown radial range, is radiation pressure dominated. At the intermediate time ($t = 10^5$) the disc, collapsed, is gas pressure dominated. The configuration at the later time ($t = 6 \cdot 10^5$), refilled, shows again a radiation pressure dominated zone up to $r = 60 R_g$.

quickly and the time on which the luminosity reduction occurs can be assumed as the instability development time. As an example, we can see the comparison between the two times in the case 'b'. The theoretical instability development time, t_{th} , can be calculated from the instability development rate Ω_{th} , given by $\Omega_{th} = \alpha\omega \frac{6(5\beta_r - 3)}{A(\beta_r)}$, with $A(\beta_r) = 8 + 51\beta_r - 3\beta_r^2$ and ω equal to the angular velocity of the disc at the radius considered (Shakura & Sunyaev 1976). With this expression for Ω_{th} we can calculate the instability development time t_{th} as $t_{th} = \frac{1}{\Omega_{th}}$. The value of t_{th} at the innermost radii is of the order of 10^{-1} sec. From the luminosity time behavior we deduce similar values.

Fig. 12 shows the ratio of the radiation pressure to the gas pressure versus the radial distance for the case 'b' when the disc was in the initial configuration, in the collapsed state (time $t = 1 \cdot 10^5$) and when it was in the refilled state (time $t = 6 \cdot 10^5$). It is clear that, in the A zone, the refilled state has a P_{rad}/P_{gas} value larger than 1, but smaller than the very initial value, at time $t = 0$. The presence of this zone with $P_{rad} > P_{gas}$ also in the refilled configuration suggests that the Shakura-Sunyaev instability may be again operating to produce the recurrent flaring activity.

The refilling time-scale computed from the simulation data is about $5 \cdot 10^5$, that is shorter than the theoretical drift time-scale due to the viscosity. We argue that the refilling is driven not only by the viscosity: also the wave phenomenon may play significant role. Indeed the plain theoretical model predicts a time-scale $t_{drift} = r^2/\nu = 1.8 \cdot 10^7$. This fact should be taken into account developing theoretical models of recurrent flaring disc activity due to refilling.

5 CONCLUSIONS

The results of our simulations of the time evolution of αP_{tot} disks, with a large portion in radiation pressure dominating conditions, show definitely that the Shakura-Sunyaev collapse instability develops. After a long time the disc recovers partially its luminosity and furthermore it exhibits a flaring like activity. The recovery time-scale is shorter than the viscous drift time-scale. We attribute to the advective-convective heat transfer a significant role to determine both the recovery and the not occurrence of the expansion instability.

We suggest that the reason for which we see no expansion instability is the presence of a radial convective motion, that isn't considered in the Shakura and Sunyaev analysis, but is naturally simulated by our code. In such conditions, the radial heat transfer due to the advection of matter (and thermal energy) carries the excess of energy produced by viscosity (that would cause the thermal expansion) away from the disc element at that r . These results imply some problem for the model of the formation of the comptonization cloud supposed to exist in many disc configurations to explain the observed radiation spectra. From the canonical disc it seems impossible to produce that comptonization cloud via the plain Shakura-Sunyaev instability.

Another relevant aspect of our simulations is the presence of acoustic waves; they can cause a kind of periodical variability of the radiation spectrum and intensity that could be related, from the observational point of view, with the phenomenon of QPOs (Psaltis 2001). Oscillation frequencies of the radiative flux we calculated are compatible with some QPOs. It is true that the total disc luminosity takes into account the contributions from the whole disc and so the wave phenomenon may not appear. However one should take also into account the possibility that the reflection of the radiation coming from inner disc zones by outer zone waves could produce an enhanced oscillation in the total luminosity. Such a study requires an accurate treatment of the interaction between the emitted radiation and the disc itself and of the radiation transfer in the outermost layers of the disc, that is beyond this contribution.

The flaring activity could be also responsible of QPO phenomena. We are planning to confirm and study its characteristics by numerical simulations with increased spatial resolution.

REFERENCES

- Abramowicz M.A., Czerny B., Lasota J.P., Szuszkiewicz E., 1988, ApJ, 332, 646A
- Agol E., Krolik J., Turner N.J., Stone J.M., 2001, ApJ, 558, 543A
- Bisnovatyi-Kogan G.S., Blinnikov S.I., 1977, A&A, 59, 111
- Brookshaw L., 1994, Mem.S.A.It., 65, n. 4, 1033
- Chakrabarti S.K., Molteni D., 1993, ApJ, 417, 671
- Chandrasekhar S., 1961, Hydrodynamic and Hydromagnetic Stability, Clarendon Press, Oxford
- Dilts G.A., 1996, Los Alamos National Laboratory Report LA-UR, 96-134
- Eggum G.E., Coroniti F.V., Katz J.I., 1987, ApJ, 323, 634
- Fujita M., Okuda T., 1998, PASJ, 50, 639

- Milsom J.A., Taam R.E., 1996, MNRAS, 283, 919
Milsom J.A., Taam R.E., 1997, MNRAS, 286, 358
Molteni D., Gerardi G., Valenza M.A., Lanzafame G., Ed. by Chakrabarti S.K., 1998, Observational Evidence for Black Holes in the Universe, Kluwer A.P., Dordrecht
Monaghan J.J., 1985, Comp. Phys. Repts., 3, 71
Nelson R.P., Papaloizou J.C.B., 1994, MNRAS, 270, 1N
Paczynski B., Wiita P.J., 1980, A&A, 88, 23
Psaltis D., 2001, AdSpR, 28, 481
Shakura N.I., Sunyaev R.A., 1973, A&A 24, 337
Shakura N.I., Sunyaev R.A., 1976, MNRAS, 175, 613
Shakura N.I., Sunyaev R.A., Zilitinkevich S.S., 1978, A&A, 62, 179
Shapiro S.L., Lightman A.L., Eardley D.M., 1976, ApJ, 204, 187
Sunyaev R.A., Titarchuk L., 1980, A&A, 86, 121S
Taam R.E., Lin D.N.C., 1984, ApJ, 287, 761

Figure captions

- Fig. 1. The r - z profile of the disc of case 'a' is shown at the time $t = 282 R_g/c$. Every SPH particle is represented by a small dot. On the x axis the r values in units of R_g are represented. On the y axis the z values in units of R_g are represented.
- Fig. 2. The r - z profile of the same disc case 'a' at the time $t = 12000 R_g/c$ is shown.
- Fig. 3. The ratio P_{rad}/P_{gas} at the times $t = 282$ and $t = 12000$ is shown. On the x axis the r values in units of R_g are represented. The configuration at the later time, collapsed, exhibits a gas pressure dominated zone up to $r = 70 R_g$, whereas the other configuration, at a earlier time, shows that, up to $150 R_g$, the disc is radiation pressure dominated.
- Fig. 4. The time behavior of the disc luminosity is shown. On the x axis the time values in units of R_g/c are represented. On the y axis the luminosity values in units of $erg sec^{-1}$ are represented.
- Fig. 5. The time behavior of the disc luminosity is shown for the disc of case 'b'.
- Fig. 6. The border particles of the disc case 'c' are shown at the times $t = 0$ (vertical crosses), $t = 20000 R_g/c$ (diagonal crosses) and $t = 22400 R_g/c$ (asterixes).
- Fig. 7. The radiative, convective and heating time-scales, ordered from the bottom to the top of the figure, are shown versus r . On the y axis the time values in units of R_g/c are represented.
- Fig. 8. The convective and advective fluxes at $r = 30 R_g$ are shown versus time. On the y axis the fluxes values in units of $erg sec^{-1} cm^{-2}$ are represented. The dashed line represents the convective flux behavior, whereas the continuous one refers to the advective flux.
- Fig. 9. The convective and advective fluxes at $r = 80 R_g$ are shown versus time. On the y axis the fluxes values in units of $erg sec^{-1} cm^{-2}$ are represented. The dashed line represents the convective flux behavior, whereas the continuous one refers to the advective flux.
- Fig. 10. The radial speed of the disc parcels is shown versus r . On the y axis the speed values in adimensional units are represented.
- Fig. 11. The vertical speed of the disc parcels is shown versus r . On the y axis the speed values in adimensional units are represented.
- Fig. 12. The ratio P_{rad}/P_{gas} in the initial configuration (asterixes) and at the times $t = 10^5$ (diagonal crosses) and $t = 6 \cdot 10^5$ (vertical crosses) is shown. The initial configuration, in the shown radial range, is radiation pressure dominated. At the intermediate time ($t = 10^5$) the disc, collapsed, is gas pressure dominated. The configuration at the later time ($t = 6 \cdot 10^5$), refilled, shows again a radiation pressure dominated zone up to $r = 60 R_g$.